ChemPubSoc Europe

DOI: 10.1002/open.201900337

Open Access ChemistryOPEN Reviews

Special Collection

# Halogen Bonding in Two-Dimensional Crystal Engineering

Joan Teyssandier, Kunal S. Mali,* and Steven De Feyter*[a]

*Dedicated to the 80th birthday of Frans C. De Schryver and Jean-Marie Lehn*

Halogen bonds, which provide an intermolecular interaction with moderate strength and high directionality, have emerged as a promising tool in the repertoire of non-covalent interactions. In this review, we provide a survey of the literature where halogen bonding was used for the fabrication of supramolecular networks on solid surfaces. The definitions of, and the distinction between halogen bonding and halogen-halogen interactions are provided. Self-assembled networks formed at the solution/solid interface and at the vacuum-solid interface, stabilized in part by halogen bonding, are discussed. Besides the broad classification based on the interface at which the systems are studied, the systems are categorized further as those sustained by halogen-halogen and halogen-heteroatom contacts.

## 1. Introduction

Two-dimensional (2D) crystal engineering is the design and fabrication of single molecule thick crystalline layers of organic and metal-organic building blocks physisorbed on solid surfaces. Recent years have witnessed rapid progress in this field largely due to fundamental interest in understanding how supramolecular interactions influence the arrangement of molecules on solid surfaces. Given that principles of supramolecular chemistry are increasingly becoming the foundation of most bottom-up fabrication strategies, significant efforts have been directed towards understanding and controlling molecular self-assembly at solid interfaces.[1]

One of the reasons behind the popularity of 2D crystal engineering in recent years is arguably the development and widespread use of scanning probe microscopy, especially scanning tunneling microscopy (STM). STM allows direct visualization of self-assembled monolayers adsorbed on solid surfaces at sub-nanometer resolution. It uses a sharp metallic tip that raster scans the surface using a piezoelectric module. Since the tip-surface distance is only a few angstroms, ultra-flat surfaces where corrugations do not exceed atomic height are preferred. The substrate surface also needs to be conductive, since the measured signal is in the form of a tunneling current. The tunneling current that flows between the tip and the surface upon application of a potential gradient, gets modified by nanoscale surface features. Both topography as well as electronic features contribute to the contrast in STM images.[2]

Other surface science techniques such as low-energy electron diffraction (LEED),[3] grazing-incidence small-angle scattering (GISAS),[4] and related in-plane X-ray and neutron diffraction techniques[5] also offer structural insights into nanostructured organic thin films. These measurements however often provide space averaged information over large areas. Such averaging may lead to loss of local imperfections. On the contrary, STM probes the surface locally and provides detailed structural information irrespective of whether the network is crystalline or amorphous. It is a versatile technique that can be used in a range of different environments such as ultra-high vacuum (UHV), air, water, gases, aqueous electrolytes and organic solvents. It can be operated in temperatures ranging from ~4 K up to a few hundred Kelvin. UHV offers ultra-clean environment that is essential to quantify supramolecular interactions which are relatively difficult to fathom in the solution phase. On the other hand, solution phase STM offers a real-life scenario, where dynamic self-assembly processes can also be studied, albeit on relatively slow time scales. STM data provides a direct visual cue to the self-assembled system and thus has the added advantage of immediate aesthetic appeal where one can directly 'see' the structure of the self-assembled system.[6]

In a typical STM experiment, molecules are deposited onto a solid surface either *via* sublimation, typically for experiments carried out under UHV conditions or from the solution phase, when the STM imaging is carried out under ambient conditions at the air/solid or liquid/solid interface. A combination of intermolecular and interfacial interactions leads to (often) spontaneous self-assembly of the building blocks on the solid surface. Similar to bulk crystallization, a delicate balance between kinetic and thermodynamic factors governs the structure formation. These factors differ significantly for systems deposited *via* sublimation and those self-assembled at the solution/solid interface. The solution/solid interface provides relatively more dynamic environment to the assembly process where there is often a free exchange between molecules already adsorbed on the surface and those present in super-

[a] *Dr. J. Teyssandier, Dr. K. S. Mali, Prof. S. De Feyter*
*Division of Molecular Imaging and Photonics*
*Department of Chemistry*
*KU Leuven-University of Leuven*
*Celestijnenlaan 200F*
*3001 Leuven (Belgium)*
*E-mail: kunal.mali@kuleuven.be*
*steven.defeyter@kuleuven.be*

Special Collection *An invited contribution to a Special Collection dedicated to Functional Supramolecular Systems*

natant solution. Such reversible adsorption-desorption dynamics allows healing of defects which enables formation of defect-free monolayers at room temperature. Such reversibility in non-covalent bond formation is the hallmark of physisorbed monolayers formed at the solution/solid interface. These dynamic processes however also increase the complexity of self-assembly relative that occurring under UHV conditions. The absence of solvent and thus the resultant lack of dynamic exchange renders the self-assembly at the UHV/solid interface relatively simple compared to that at the solution/sold interface.

In contrast to traditional crystal engineering where crystallization occurs in 3D, self-assembly of molecules in 2D is expected to present a relatively simpler crystallization scenario, both structurally and mechanistically. However, presence of a solid surface, which is rarely an innocent partner, complicates the 2D crystallization processes due to the presence of interfacial interactions. Molecule-substrate and solvent-substrate interactions are known to strongly influence the outcome of self-assembly on solid surfaces as they can compete with intermolecular interactions. Moreover, the strength of molecule-substrate interactions varies drastically depending of the type of molecules and the substrate involved in the process. It is well known that organic molecules often exhibit specific 'epitaxial' relationship with the substrate surface such that the adsorption site and geometry is defined by the substrate lattice. Typically, molecule-substrate interactions determine the initial adsorption conformation when the intermolecular interactions are relatively weak (van der Waals interactions, dispersive forces) which then control the subsequent network formation. Strong, directional intermolecular interactions such as hydrogen bonding and metal-ligand co-ordination govern the structure formation to a large extent, however even in such cases, the influence of the underlying substrate cannot be neglected.

A substantial part of the research on 2D crystal engineering deals with exercising precise control over intermolecular and interfacial interactions *via* molecular design and surface supramolecular chemistry approaches, respectively. With such control, the composition and positioning of molecular building blocks in (multicomponent) self-assembling systems can be controlled. Similar to that in solution phase and in the solid state, the basis of self-assembly on solid surfaces remains molecular recognition. In this process, molecules recognize other molecules and bind with them *via* non-covalent interactions. Traditionally a wide range of intermolecular interactions such as hydrogen bonds,[7] van der Waals forces,[8] metal-ligand,[9] dipole-dipole[10] and π-π stacking interactions[11] have been employed to design and fabricate increasingly complex (multicomponent) supramolecular architectures. The interactions listed above vary in strength as well as directionality however they need to be considered slightly differently in the context of 2D self-assembly. This is because certain interactions, such as van der Waals forces between alkyl chains are not considered directional in a conventional sense, however in presence of a substrate such as highly oriented pyrolytic graphite (HOPG), it is possible to use them in a highly directional manner thanks to the interactions that exist between the graphite lattice and alkyl chains.[12]

Somewhat recent addition to the repertoire of non-covalent interactions employed in 2D crystal engineering is halogen bonding. While the surface-based self-assembly of halogenated compounds has been studied for many years, only recently halogen-bonding in its true sense (*vide infra*) has been employed as a tool for 2D crystal engineering. This review highlights fundamental aspects of halogen bonding and discusses halogen-bonded supramolecular networks. Systems that employed halogenated compounds for 2D crystal engineering are also surveyed. The first part provides the definition of a halogen bond and touches upon the unique features of covalently bonded halogen atoms that are responsible for halogen bonding. Similarities and differences between halogen and hydrogen bonding are outlined. The second part discusses

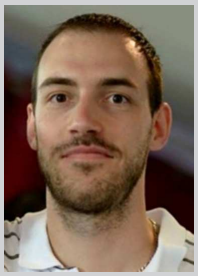

Dr. Joan Teyssandier obtained his Ph.D. in chemistry in 2012 from the University of Paris Diderot (France) under the supervision of Dr. Philippe Lang. During his doctoral work he studied the growth and properties of molecular and metallic guests confined in nanoporous supramolecular networks. Thereafter, he joined the group of Prof. Anna Proust at the University Pierre and Marie Curie for a postdoctoral position to study functionalized polyoxometalates for surface nanostructuration. He has been a postdoctoral fellow in the De Feyter group at KU Leuven since 2014, where his research involves investigating supramolecular self-assembly on surfaces and functionalization of 2D materials.

Dr. Kunal S. Mali obtained his Ph.D. in chemistry in 2008 from University of Mumbai (India) under the supervision of Dr. G. B. Dutt. His doctoral work focused on investigation of fast dynamic processes in complex media by employing time-resolved fluorescence spectroscopy. Currently, he is a research manager at KU Leuven in the De Feyter group where his research involves different aspects of surface-confined supramolecular self-assembly and surface functionalization.

Prof. Steven De Feyter is a professor at KU Leuven in Belgium. After completing his Ph.D. with Frans De Schryver at KU Leuven in 1997, he moved for a postdoctoral position to the group of Ahmed Zewail (California Institute of Technology, Pasadena). His research group investigates various aspects of supramolecular chemistry and self-assembly phenomena of surfaces using scanning probe methods with special attention to liquid-solid interfaces.

recent reports where halogen-halogen and/or halogen-heteroatom interactions were employed for the fabrication of supramolecular architectures at the solution/solid interface. This discussion is followed by summary of systems formed under UHV environment. The final part of the review summarizes the discussion and provides future perspectives.

## 2. The Halogen Bond

Despite being already known for a couple of centuries, halogen bonding received its formal definition relatively recently. IUPAC defined halogen bonding in 2013 as follows:

"*A halogen bond occurs when there is evidence of a net attractive interaction between an electrophilic region associated with a halogen atom in a molecular entity and a nucleophilic region in another, or the same, molecular entity.*"[13]

At first sight, the ability of halogens to serve as the electrophilic bonding partner appears rather perplexing. Due to their strong electronegativity, halogen atoms are usually considered as the sites of high electron density and thus the idea of an attractive interaction between them and a nucleophile seems somewhat counterintuitive. Nevertheless, the origin of electrophilicity can be traced back to the anisotropic distribution of electronic density of covalently bonded halogens. When a halogen atom forms a covalent bond with other element (for example, carbon-halogen, C–X bond), the electron density is depleted in its outermost region along the extension of the C–X bond axis and gets concentrated in the direction perpendicular to the C–X axis. Thus, the halogen atom becomes oblate showing a characteristic polar cap with positive electrostatic potential and an equatorial belt with negative electrostatic potential. This process is called *polar flattening* and represents a general behavior that is also shown by other elements. The electrophilic polar cap is called *σ-hole* as it is seen as the local deficit of electron density opposite a σ-bond. The *σ-hole* interacts with nucleophiles and the equatorial electron rich belt interacts with electrophiles. The focused nature of the *σ-hole* thus explains the high directionality exhibited by halogen bonds wherein the nucleophiles typically interact with the halogen atom in a linear (180°) fashion whereas electrophiles interact laterally (Figure 1a).[14]

Halogens can be involved in hydrogen bonding, where they act as Lewis bases (interaction energies up to 140 kJ/mol) and the strength of hydrogen bonds involving halogens varies as $F > Cl > Br > I$.[15] Alternatively, they form halogen bonds acting as Lewis acids with an opposite trend in bond strength as compared to hydrogen bonds, namely $I > Br > Cl \gg F$. This trend relates to the strength of the *σ-hole* which in turn depends on the electron-withdrawing ability of the group to which the halogen atom is bonded and on the polarizability of the halogen atom itself.[14a,16] Fluorine being the least polarizable of halogens can act as halogen bond donor only when it is attached to strong electron withdrawing groups.[17] The energy of the halogen bonds typically ranges from 5–30 kJ/mol, but in exceptional instances, such as in the case of $I^-$–$I_2$ interactions in $I_3^-$ anion, up to 180 kJ/mol. It must be noted that halogen bonding addresses only those intermolecular contacts where the halogen atoms function as electrophiles (Lewis acids) and interact with nucleophiles (Lewis bases) at the pole. Halogens are also involved in halogen-halogen interactions which, depending on their geometry, are classified as either type-I

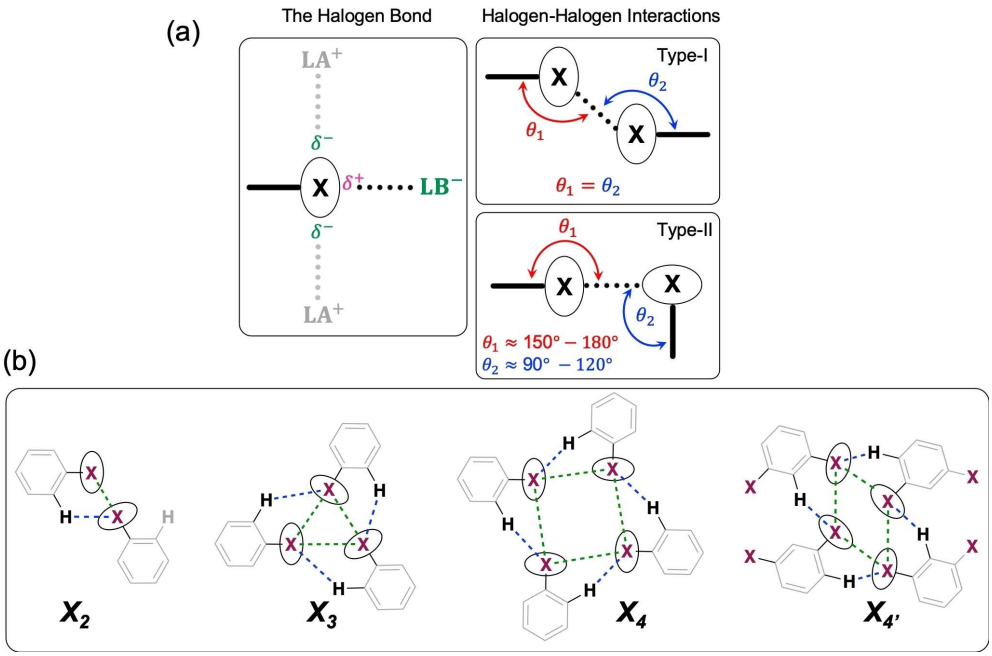


**Figure 1.** (a) Schematic showing the halogen bond and halogen-halogen interactions. X = halogen atom, $LB^-$ = Lewis base, $LA^+$ = Lewis acid. Almost all halogen-heteroatom contacts and many halogen-halogen contacts qualify as halogen bonds (b) Different motifs involving type-II halogen-halogen contacts discussed in this review. These are similar to the $X_2$, $X_3$, $X_4$ synthons however in the examples discussed in this review, often accompanied by hydrogen bonds (blue dotted lines) besides the type-II halogen-halogen contacts (green dotted lines).

(symmetrical) or type-II (bent) (Figure 1). Almost all halogen-heteroatom contacts and many halogen-halogen contacts qualify as halogen bonds.[18]

Although halogen bonding is rapidly evolving as a routine and predictable tool in supramolecular chemistry, hydrogen bonding remains arguably the most predominantly encountered noncovalent interaction in molecular recognition processes. There are a number of similarities between the two interactions. Both are attractive interactions that involve donation of electron density from a nucleophilic moiety (halogen/hydrogen bond acceptor) to an electrophilic moiety (halogen/hydrogen). Both interactions are highly directional. In fact, halogen bonds are expected to be more directional than hydrogen bonds due to the highly focused nature of $\sigma$-*hole* along the *R–X* bond axis as described earlier. The strength of both these noncovalent interactions is readily tunable by changing the functional group attached to the hydrogen-halogen atom. While it is readily accepted that the hydrogen bond is relatively stronger intermolecular interaction than the halogen bond, under certain conditions, the halogen bond can be of comparable strength or even stronger than typical hydrogen bonds.[19] There exist some stark differences as well. Since halogen atoms are hydrophobic, a typical halogen bonding donor site is significantly less hydrophilic compared to a typical hydrogen bond donor site. Given the other similarities between them, halogen bonds thus can be considered as hydrophobic analogues of hydrogen bonds. An important difference between the two types of interactions arises due to the size of the constituent atoms. Since the halogen atoms are larger in size than hydrogen, halogen bonding is relatively more sensitive to steric hindrance compared to hydrogen bonding.[16] It is also known that under certain conditions hydrogen and halogen bonds compete with each other[20] and under certain other conditions they augment each other. For example, it has been recently demonstrated that a hydrogen bond to the nucleophilic belt of a halogen atom increases its potential to act as a halogen bond donor.[21]

## 3. Halogen-Halogen Interactions and Halogen-Bonding in Self-Assembled Networks

As mentioned earlier, halogen bonding is a relatively new addition to the tenets of 2D crystal engineering. While a number of concepts/modules already established in bulk crystal engineering can be readily applicable on surface, differences do exist due to presence of the substrate. A number of initial studies involved supramolecular networks which, together with halogen-halogen interactions, were sustained by additional van der Waals interactions between neighboring molecules. It must be noted that if the halogen-halogen distance is not smaller than the sum of van der Waals radii of the interacting halogens, then the existence of halogen bonding is questionable. A survey of recent literature reveals that there is a tendency to term halogen-halogen contacts, especially type-I contacts, as halogen bonds and thus more discretion should be used in the usage of the term *halogen-bonding* for such intermolecular interactions. More recently however, self-assembled 2D networks entirely sustained by halogen bonds have been fabricated on solid surfaces (*vide infra*). In order to ensure fabrication of supramolecular networks truly sustained by halogen bonds, careful design of the assembling units is essential such that the on-surface self-assembly is mostly governed by the targeted halogen bonding interactions.

In the following sections we survey the published literature and discuss the self-assembly of halogenated building blocks using different examples. The discussion is classified based on whether halogen bonds are formed *via* homomeric interactions (halogen-halogen contacts) or through heteromeric pairs (halogen-heteroatom contacts). These sections are further classified based on whether the self-assembled networks are formed at the solution/solid or at the vacuum/solid interface.

### 3.1. Halogen-Halogen and Halogen-Heteroatoms Interactions at the Solution/Solid Interface

One of the early examples of halogen-bonded 2D supramolecular network characterized by STM at the solution/solid interface consisted of a tetrabrominated derivative of an organic semiconductor, tetrathienoanthracene (**1**, Figure 2a).[22] **1** self-assembles at the 1,2,4-trichlorobenzene (TCB)/HOPG interface to form a close-packed network with an oblique unit cell (Figure 2b). The molecules arrange in slip-stacked columns which are stabilized through Br···S and Br···H interactions along the column axis and *via* Br···Br and Br···H interactions laterally (Figure 2c). DFT calculations revealed that the distances between the intermolecular contacts mentioned above are shorter than the sum of their van der Waals radii. In particular, the Br···Br distance was found to be much shorter (3.42 Å) and at the lower end of the 3.4–3.9 Å range found for Br···Br contacts in organic crystals. These values in conjunction with the observed geometry for the contacts, indicate the formation halogen bonds which constitute the primary driving force of the assembly of **1**. However, the contribution of van der Waals, and hydrogen bonding interactions to the stabilization of the network was non-negligible, and the halogen bonds were always found to be a part of triangular binding motifs consisting of either Br···Br···H or S···Br···H contacts.

The electrostatic potential map (ESP) indicated that the $\sigma$-*hole* of one bromine atom points towards the equatorial electron rich belt of a bromine atom on a neighbouring molecule leading to a Br···Br halogen bond (D1, Figure 2d). The same bromine atom points with its nucleophilic ring towards a hydrogen atom leading to a Br···H hydrogen bond (D4, Figure 2d). The Br atom at the long side of **1** points with its electronegative ring towards the hydrogen forming Br···H hydrogen bond (D5, Figure 2e). Furthermore, the $\sigma$-*hole* of the bromine atom reaches out towards an electron lone pair on one S atom (D2, Figure 2e) indicating formation of a Br···S halogen bond. This analysis is in line with the propensity of halogens to interact with nucleophiles in a linear fashion along the $\sigma$-*hole*, and with electrophiles laterally *via* the equatorial

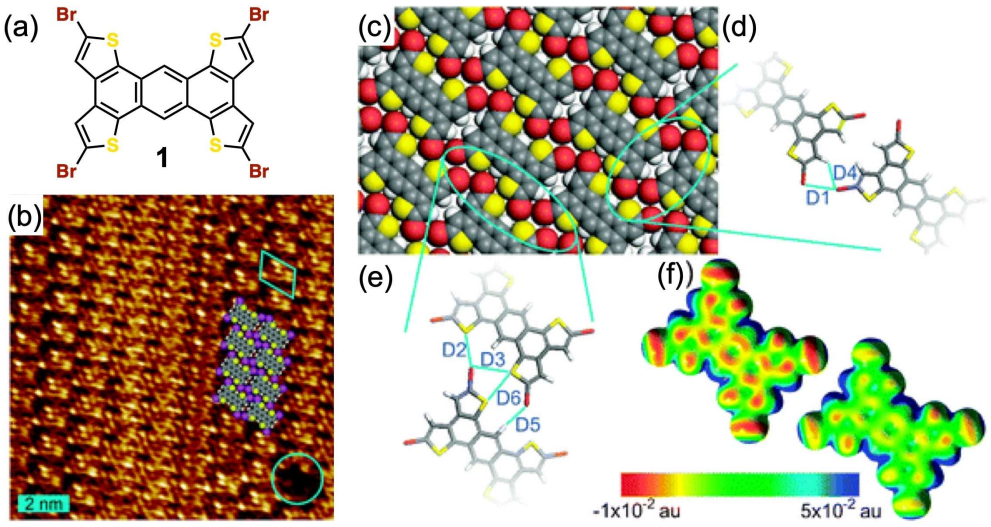


**Figure 2.** (a) Molecular structure of **1**. (b) STM image of the monolayer formed by **1** at the TCB/HOPG interface. (c) DFT optimized structure of the network. In the molecular model, carbon: grey, hydrogen: white, bromine: red, sulphur: yellow. (d, e) Intermolecular contacts along the short (d) and the long (e) side of the molecule. (f) ESP map of **1** in vacuum (left) and when adsorbed in the monolayer (right). Reproduced from ref. [22] with permission from the Royal Society of Chemistry.

nucleophilic ring as described earlier. Comparison of the ESP of an isolated molecule with that of a molecule in the self-assembled network revealed significant changes in molecular polarization upon close packing. The formation of very large domains ($>1\ \mu m^2$) indicated the faster dynamics at the solution/solid interface promoted by relatively weaker halogen bonds which accelerate growth and Ostwald ripening.[22]

Since halogenation of organic semiconductors lowers their electronic band gap, there is significant interest in understanding the influence of halogen bonding interactions on the network structures of organic thin films. One of the approaches involves changing the molecular design *via* synthesis of structurally similar derivatives such that intermolecular interactions are modified and then comparing the thin films of such materials for their structure as well as function. Following up the work described above, it was shown how the changes in molecular design within this family of molecules influenced the structure of self-assembled monolayers. It was concluded that a halogen-halogen and hydrogen-halogen three-centre binding motif (see Figure 2d) where the H-bond is formed almost orthogonally to the halogen-bond is the basis of self-assembly of this family of compounds.[23]

The fact that the surface and the solvent matters, and quite significantly so, was illustrated by comparison of self-assembly of 2,4,6-tris(4-iodophenyl)-1,3,5-triazine (**2**, inset Figure 3a) and 2,4,6-tris(4-bromophenyl)-1,3,5-triazine (**3**, inset Figure 3c) on HOPG and on Au(111).[24] It was originally intended that by changing the type of halogen, molecule-substrate interactions can be modulated, and thus one would observe differences in packing of these two molecules. However, both molecules formed similar close-packed assemblies on HOPG, which are stabilized by a combination of halogen···halogen interactions and halogen···H hydrogen bonds. Gas-phase DFT calculations performed on both systems revealed that, although the molecular configuration positions the $\sigma$-*hole* of the halogen atoms towards the nucleophilic belts of neighbouring C–X bonds (d1, Figure 3b, 3d), the halogen atoms remained too far apart to engage in halogen bonding. In absence of halogen bonding interactions, the molecules within the rows (rectangle, Figure 3b, 3d) and between neighbouring rows (oval, Figure 3b, 3d) are mostly stabilized by aromatic C–H···X hydrogen-bond contacts. Furthermore, though the $\sigma$-hole of the halogen atom points toward the nitrogen atom of the neighbouring molecules along the *v*-vector (dotted line, Figure 3b, 3d), its approach to the triazine core is obscured by the hydrogen atoms of the phenyl groups (d2, Figure 3b, 3d). As a result, the nitrogen atoms do not contribute to the lateral stabilization of the assembly. The only difference in the assemblies of **2** and **3** on HOPG comes from hydrogen bonds involving the halogen atoms. DFT calculations clearly indicated that the halogen···hydrogen contacts are shorter in the case of the brominated compound **3** than those for the iodinated derivative **2**, as expected on the basis of stronger C–Br dipole.

It must be noted that the self-assembly of **2** and **3** was studied from TCB and 1-phenyloctane solutions, respectively due to the lack of self-assembly of **3** from TCB. No indication of solvent co-adsorption was observed in the two solvents mentioned above. However, when the self-assembly is carried out from heptanoic acid, a completely different topology was observed (Figure 3e). The network formed at the heptanoic acid/HOPG interface consists of co-adsorbed solvent molecules that completely 'insulate' the assembling molecules of **3** from each other. DFT calculations revealed that heptanoic acid molecules form cyclic hydrogen-bonded hexamers and co-adsorb in between the molecules of **3** (Figure 3f).

On the surface of Au(111) however, rather complex self-assembly behaviour was observed. The two halogenated compounds behave differently. Compound **3** leads to formation

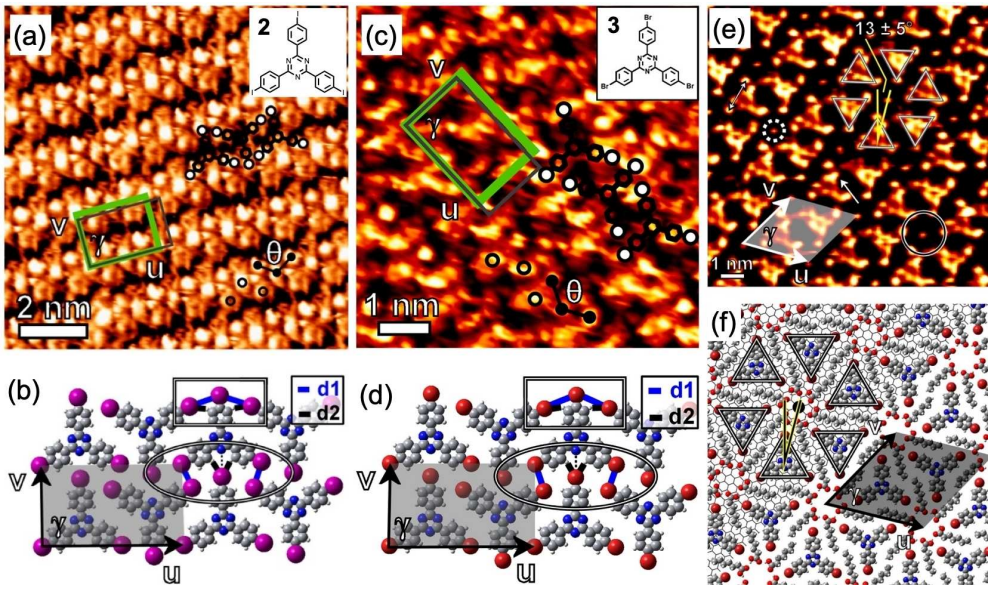


**Figure 3.** (a) Self-assembled network formed by **2** at the TCB/HOPG interface. The inset shows the molecular structure of **2**. (b) DFT calculated structure of the network. The iodine-iodine and iodine-hydrogen contacts are denoted by d1 and d2, respectively. (c) Self-assembled network formed by **3** at the 1-phenyloctane/HOPG interface. The inset shows the molecular structure of **3**. (d) DFT calculated structure of the network. (e) Self-assembled network formed by **3** at the heptanoic acid/HOPG interface. The grey triangles highlight molecules of **3**. The dark area in between the molecules is occupied by molecules of the solvent. (f) DFT calculated model for the two-component monolayer showing co-adsorption of heptanoic acid. Reproduced from ref. [24] with permission from the American Chemical Society.

of two different phases on differently reconstructed regions of the Au substrates. The difference in molecular packing plausibly arises from the difference in surface potential between the hcp- and fcc-stacked zones further illustrating how sensitive the molecules can be to interactions with the substrate. On the contrary, **2** formed a similar network on Au(111) as that on HOPG.

The concentration dependence of molecular self-assembly on solid surfaces has been well-documented over the years. A number of alkyl-substituted[25] and hydrogen bonding[26] building blocks are known to exhibit concentration dependent networks on solid surfaces. Typically, densely packed networks are obtained from concentrated solutions whereas dilute solutions yield low-density or so-called nanoporous networks. The fact that halogenated building blocks also show concentration-dependent assembly behaviour was demonstrated in the case of 1,3,5-tris(4-iodophenyl)benzene (**4**, Figure 4a) at the 1-phenyloctane/HOPG interface.[27] This building block forms a relatively densely packed network at relatively higher concentrations ($10^{-7}$ M, Figure 4b).

Adjacent molecules are antiparallel with respect to each other. The relative orientation of the molecules along unit cell vector '*a*' indicates a possibility of type-II halogen-halogen interactions (*σ-hole pointing towards the electron rich equatorial region,* Figure 4c) between the iodine atoms possibly amounting to halogen bonds. The chains of molecules with identical orientation are stabilized by such type-II halogen-halogen contacts and these chains are further close-packed to form a 2D network. The darker regions observed in the STM image correspond to the vacant spaces visible in the molecular model (Figure 4c) and are possibly occupied by mobile solvent molecules.

At lower concentrations ($< 10^{-9}$ M) however, a low-density network is obtained at the 1-phenyloctane/HOPG interface. Figure 4d shows the STM images of the low-density network where the iodinated ends of each molecule appear brighter compared to the rest of the molecule. A trimer motif can be readily discerned from the STM image as well as the corresponding molecular model presented in Figure 4e. This motif closely resembles the trimeric $X_3$ synthon and has been reported for bulk crystallizations[28] as well as on-surface network formation.[23,29] In the trimeric motif, the C–X···X–C bonding angle is approximately 120° indicating the possibility of the formation of halogen bonds based on type-II interactions. The open spaces within the network are occupied by mobile 1-phenyloctane molecules. The low-density network formed by **4** is one of the few examples where halogen bonding interactions appear to be structure directing in nature (*vide infra*).[27]

Variation in the position and the number of the halogen substituents on the aromatic framework also influences the outcome of the self-assembly process. This aspect was illustrated using alkoxy substituted phenanthrene derivatives.[30] Self-assembled networks formed by compounds **5**, **6** and **7** (Figure 5) at the octanoic acid/HOPG interface were compared. Both **5** and **6** form densely packed columnar networks at relatively higher concentrations. The dense columns are stabilized by van der Waals interactions between the hexadecyloxy chains and π-stacking interactions between the phenanthrene units which adsorb edge-on at higher concentration. At relatively lower concentrations, the phenanthrene units of both the molecules adsorb face-on on the HOPG surface. Self-

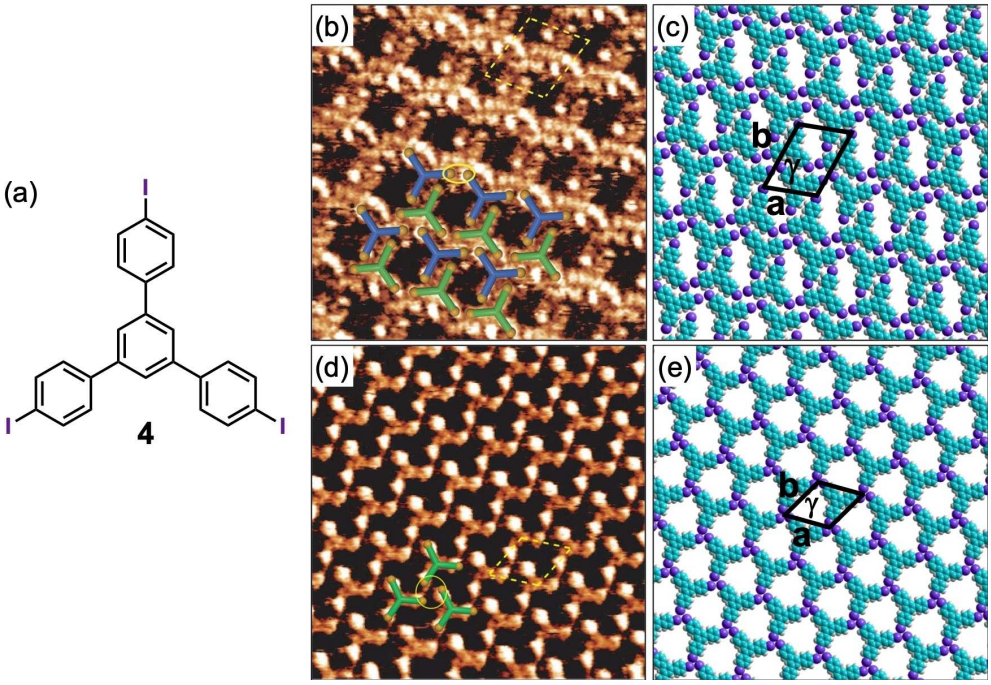


**Figure 4.** (a) Molecular structure of **4**. (b) and (c) show the STM image of the network obtained at higher concentrations ($10^{-7}$–$10^{-9}$ M) and the corresponding molecular model for the network, respectively. (d) and (e) show the STM image of the network obtained at lower concentrations ($< 10^{-9}$ M) and the corresponding molecular model for the network, respectively. Reproduced from ref. [27] with permission from the American Chemical Society.

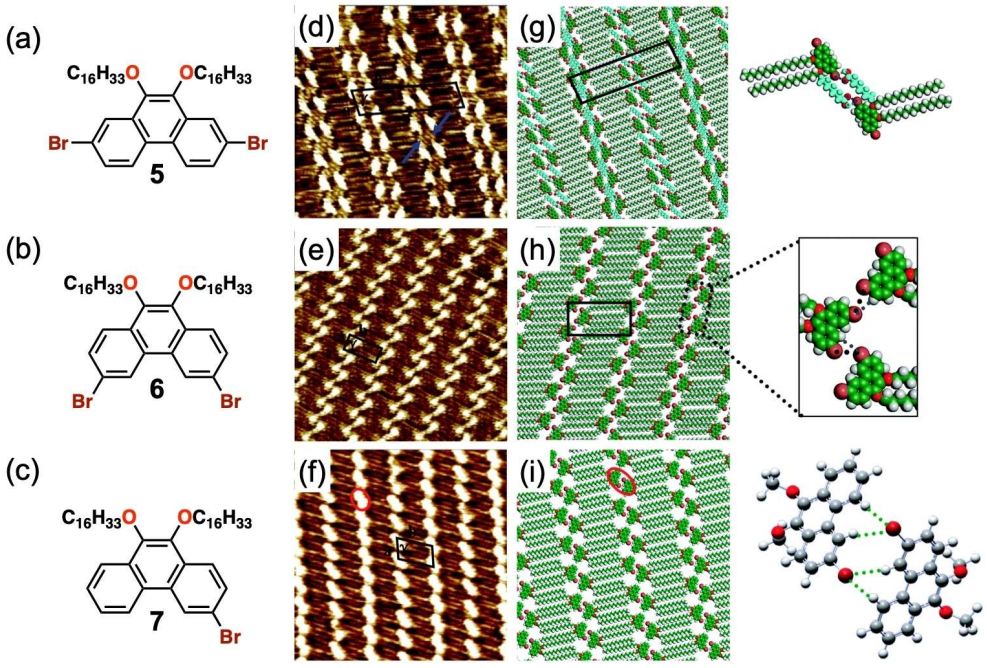


**Figure 5.** (a), (b) and (c) Molecular structures of **5**, **6** and **7**, respectively. (d), (e) and (f) Self-assembled networks formed by **5**, **6** and **7**, respectively. STM image size is $15 \times 15$ nm$^2$. Panels (g), (h), (i) present molecular models corresponding to STM images displayed on the left. Reproduced from ref. [30] with permission from the Royal Society of Chemistry.

assembly of **5** at lower concentrations leads to columnar assembly which consists of dimer rows. STM images clearly reveal that the phenanthrene units in each dimer are separated from each other such that no halogen-halogen interactions are possible (Figure 5d, g). The space in-between two phenanthrene cores is occupied by octanoic acid molecules. The solvent molecules are proposed to stabilize the dimers *via* Br···C=O halogen bonding and O–H···Br hydrogen bonding

interactions with **5** (Figure 5g). At intermediate concentrations however, **5** forms a network which consists of rows of face-on and edge-on adsorbed phenanthrene units. Halogen bond formation between adjacent face-on adsorbed phenanthrene units has been proposed. DFT calculations in vacuum were carried to understand if the Br···Br contacts qualify as formal halogen bonds. While the DFT calculations did reveal Br···Br distances shorter than the sum of their van der Waals radii, we note that the alkoxy chains were omitted from dimers for the DFT calculations. It is well-known that long alkyl chains stabilize molecular assembly *via* both interchain van der Waals interaction and interactions with the substrate. Thus, the contribution of Br···Br and Br···H contacts to the overall stabilization of the supramolecular networks could be relatively lower compared to that provided by interdigitated alkoxy chains.[30]

In contrast to compound **5**, the self-assembly of **6** at the octanoic acid/HOPG interface leads to a dense zigzag pattern without any solvent coadsorption (Figure 5e, f). This network is stabilized by pairs of Br···Br and H···Br interactions. The different position of the Br atoms on the phenanthrene units (in comparison to that in **5**) allows to create a higher density of Br···Br van der Waals contacts, in addition to H···Br hydrogen bonds. The self-assembled network formed by the monobrominated compound **7** is somewhat similar to that formed by **6** (Figure 5f, i). Similar to the results described above, the influence of the number of Br substituents on 2D self-assembly of a pyrene derivative has been reported on Au(111) surface using UHV STM carried out at room temperature.[31]

When considering the self-assembly of alkyl substituted aromatic compounds carrying halogen atoms, one must keep in mind the real contribution of halogen bonding to the structural outcome as the alkyl chains are known to strongly dominate self-assembled network formation on the surface of HOPG. Thus, special care must be exercised before attributing a certain network structure to halogen-halogen interactions or halogen bonds. Very often a given structural outcome is the result of a combination of intermolecular and interfacial interactions including geometric requirements for efficient packing. Thus, despite their highly directional nature, halogen-halogen interactions/bonds contribute only partially towards defining the structure of the self-assembled network in view of their relatively lower strength.

An interesting example in this context is the self-assembly of 1,3-dibromo-5-alkoxybenzene derivatives (**8**, Figure 6a). These building blocks are structurally simple and yet yield relatively complex self-assembled networks at the liquid/solid interface. Figure 6b shows the STM image of the monolayer formed by 1,3-dibromo-5-octadecyloxybenzene at the 1-phenyloctane/HOPG interface. The monolayer resembles a bricklayer where the bright rectangular features are attributed to the brominated phenyl rings. The network structure is rather complex despite the simple molecular design. It consists of discrete clusters of six (yellow arrow) and four molecules (blue arrow) that alternate in a regular fashion. The proportion of such hexamers and tetramers within the monolayer was found to be 1:1. A comparison of STM data with different chains lengths indicated that the alternating arrangement of hexamers and tetramers is the most favourable structure for this family of compounds. The network is stabilized by van der Waals interactions between the interdigitated alkoxy chains and type-

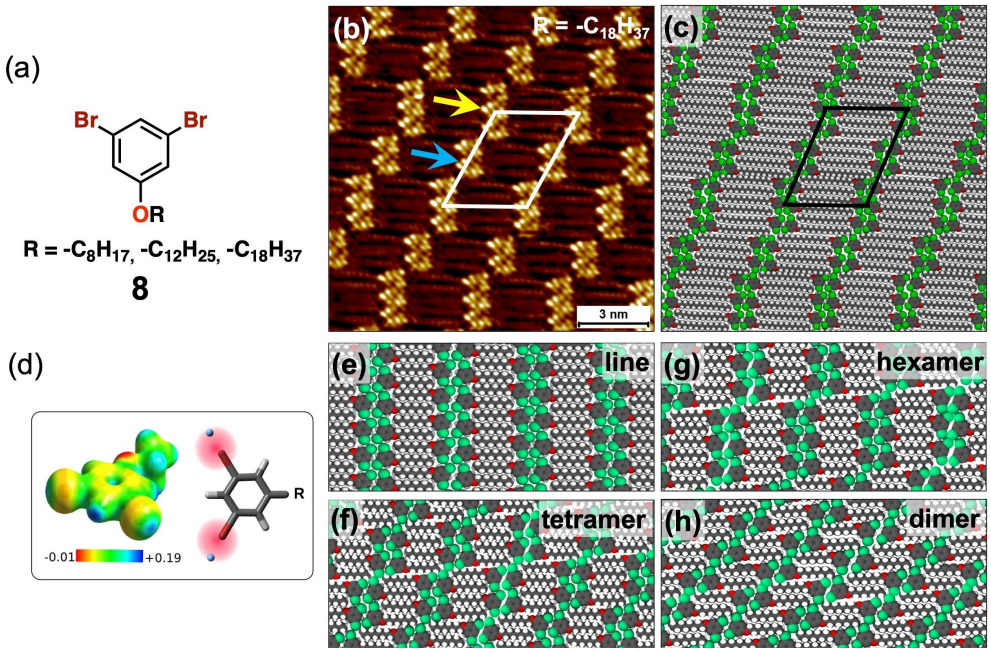


**Figure 6.** (a) General molecular structure of 1,3-dibromo-5-alkoxybenzene derivatives. (b) STM image of the monolayer formed by 1,3-dibromo-5-octadecyloxybenzene at the 1-phenyloctane/HOPG interface. (c) Corresponding molecular model. (d) Electrostatic potential map of 1,3-dibromo-5-ethoxybenzene. The *σ-hole* appears as blue coloured region together with a scheme showing the positive x-site approach used to modify the force field. (e–f) Simulated packings for experimentally observed hexamer and other hypothetical structures. Reproduced from ref. [32] with permission from the Royal Society of Chemistry.

II halogen-halogen contacts (Figure 6c). Besides the halogen-halogen contacts, hydrogen bonds between bromine atoms and the aromatic C–H groups also contribute to the stabilization of the network. This bonding motif is depicted as $X_4'$synthon in Figure 1b.[32]

It is readily understood that the discontinuity observed in the self-assembled network is neither favourable for halogen bonding nor for the van der Waals interactions between the alkoxy chains. This points towards a third factor, namely the molecule-substrate interactions. It is possible that a hypothetical continuous lamella (Figure 6e) represents a situation where the self-assembled system is strained and the discontinuity in the columns thus represents a way to release the built-up strain. In such a scenario, theoretically obtained stabilization energies for the continuous (hypothetical) and discontinuous hexameric (experimentally observed) lamellae should provide a clear indication on the stability of the networks. To carry out such calculations, a modified force field that includes an extra charged site to mimic the *σ-hole* on the halogen atom was developed (Figure 6d). Molecular mechanics calculations with such modified force field were then used to estimate the total potential energies for the experimentally observed and hypothetical networks. The total potential energies of all the networks considered for the analysis (Figure 6e–h) were found to be similar indicating that the discontinuity in the columns does not cause a significant energy penalty to the self-assembled network. The area per molecule for each simulated system was however found to decrease systematically while going from the hypothetical line structure to the experimentally observed hexamer structure. Based on this observation, it was concluded that the hexamer structure is relatively more compact compared to the hypothetical line structure. Thus, the peculiar network structure originates due to packing constraints that allow inclusion of more molecules within the same area for the fractured lamellae as compared to the continuous ones. Based on this case study, it was concluded that the type-II halogen-halogen interactions are not necessarily structure directing and when competing interactions are at play, apparently minor effects such as packing constraints become structure directing.[32]

There exist only a few examples where halogen-heteroatom interactions lead to the formation of open porous networks at the solution/solid interface. The first reported example consists of two-component porous networks formed from halogen bond donors (**11**, **12** Figure 7a) and a halogen bond acceptor carrying pyridyl moieties (**9**, Figure 7a). **11** and **12** were chosen as halogen bond donors as the electronegative fluorine atoms increase the electrophilicity of the iodine atoms which then can readily interact with the nucleophilic pyridyl nitrogen atoms of **9**. Deposition of 1-phenyloctane solutions containing a mixture of **9** and **11** however resulted in preferential adsorption of **9** and no co-assembly was observed. The halogen bonded co-assembled network was only obtained when the STM tip was preloaded with the **9** and **11** and scanned across the surface covered with 1-phenyloctane while applying voltage pulses to the STM tip. This so-called 'electrical manipulation' yielded an ordered hexagonal network with unit cell closely matching with the anticipated network featuring C–I···N halogen bonds. This remains the only example where an open porous network solely sustained by halogen bonding was formed at the solution/solid interface. Attempts to produce a network with even larger pores using a combination of **9** and **12** however failed as the system preferred to form a network with relatively smaller cavities. Besides the primary (C–I···N) halogen bonding, this network is possibly stabilized by hydrogen bonding interactions involving (C–H···F) hydrogen bonds (Figure 7c, 7g).[33] These results were later reproduced using a rather simpler experimental approach *via* premixing of solutions using

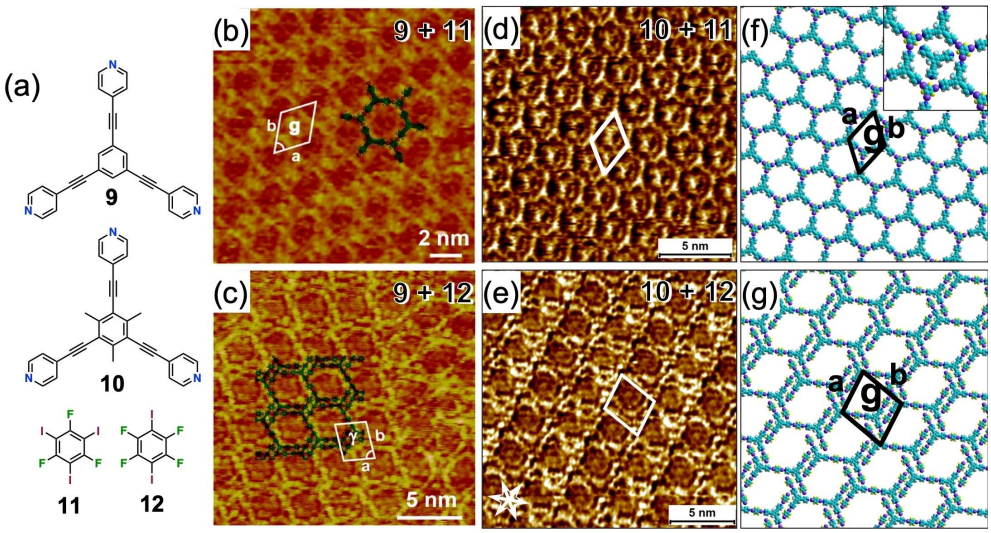


**Figure 7.** (a) Molecular structures of the halogen bond accepting (**9**, **10**) and donating units (**11**, **12**). (b) STM image of the halogen bonded porous network obtained using **9** and **11**. (c) A supramolecular network formed using a combination of **9** and **12**. This network is stabilized by halogen bonds as well as hydrogen bonds. (d) Porous network obtained using solution deposition of **10** and **11**. (f) Molecular model corresponding to the porous network obtained from **10** and **11**. The inset shows the possible immobilization of **10** within the pores of the bicomponent network. (g). Molecular model for the bicomponent system of **10** and **12**. Reproduced from ref. [26b, 33] with permission from the Royal Society of Chemistry and the American Chemical Society, respectively.

a slightly different halogen bond acceptor (**10**, Figure 7a). Two-component halogen-bonded networks (Figure 7d, e) were formed akin to those displayed in Figure 7b, c. The honeycomb network obtained using **10** as the halogen bond donor was found to contain the halogen bond acceptor as a guest molecule. The formation of an auto host-guest system in this case indicated that strength of halogen bonds in this specific case is not enough to sustain the open network and that the molecular guests are needed to stabilize the supramolecular assembly.[26b]

Another example of a porous network based on halogen-heteroatom contacts used a design similar to that displayed in Figure 7a but both the halogen bond donor (**13**, Figure 8a) and the acceptor (**14**, Figure 8a) units were substituted with additional phenyl rings carrying octadecyloxy chains. Deposition of a bicomponent solution containing appropriate ratio of **13** and **14** onto the surface of HOPG yielded a honeycomb network. The vertex of each hexagon is made up of three pairs of halogen bonded molecules of **13** and **14**. The periodicity of the network is defined by the length of the alkoxy chains which constitute the side of each hexagon extending from the halogen bond donating and accepting units. This fairly complex system was also found to exhibit organizational chirality on surface where the hexagons could be identified as clockwise (CW) and (CCW) depending on the interdigitation pattern of the chains. When a slightly different halogen bond acceptor with a different position of the pyridinic nitrogen was used, no porous networks were obtained. This observation highlighted the importance of the design aspect which is intimately related to the directional nature of halogen bonds.[34]

### 3.2. Halogen-Halogen and Halogen-Heteroatoms Interactions at the UHV/Solid Interface

As evident from the examples described so far, due to the relatively weak nature of homomeric halogen-halogen interactions, most self-assembled networks tend to adopt close-packed structures to maximize intermolecular interactions under ambient conditions. Thus, porous supramolecular networks based on halogen-halogen interactions are rarely (Figure 4) observed under ambient conditions. Such open networks however can be stabilized at lower temperatures. Since the UHV environment allows STM measurements to be carried out at temperatures as low as 4 K, there is significantly less energy available to the assembling molecules and thus even weak interactions become dominant. This also allows greater control over the surface coverage and it is possible to work with sub-monolayer coverages. Furthermore, the absence of solvent and thus in turn the absence of molecule-solvent and substrate-solvent interactions reduces the complexity of self-assembly processes occurring under UHV environment compared to those at the solution/solid interface. Lastly, due to the simplicity of the interface it is relatively straightforward to assess the co-operative and/or competitive role of halogen-halogen interactions with other intermolecular interactions as demonstrated in the examples described below.

An example of concerted hydrogen and halogen bonding interactions was reported for the self-assembly of 4,4″-dibromo-p-terphenyl (**15**, Figure 9a) on Ag(111) surface under UHV conditions. **15** forms porous networks with either square (Figure 9b), rectangular (Figure 9c) or hexagonal (Figure 9d) pores. The vertices of all the motifs consist of Br···Br contacts. The square and the rectangular polymorphs consist of the molecules connected through quadrupole nodes. Each Br atom acts as a halogen bond donor and acceptor through a type-II Br···Br contact while simultaneously involved in a hydrogen bonding interaction with the hydrogen atom of the aromatic –C–H group as depicted in Figure 9g. The hexagonal pores, on the other hand, are formed *via* $X_3$-synthons which are further supported by Br···H bonds. The three networks are thus stabilized by a combination of halogen and hydrogen bonding.[35]

Deposition of **15** on Au(111) yielded only the rectangular network based on $X_4$-synthons (Figure 9e). Interestingly, its longer analogue, (**16**, Figure 9a) only formed the square pores and no rectangular ones where observed at the UHV/Au(111) interface (Figure 9f). This difference was rationalized by considering the differences in molecule-substrate interactions and possible atomic registry effects of molecules on Au(111). At higher surface coverages, a denser ladder-like structure with triple nodes was observed for both **15** and **16**. This network was only supported by Br···H hydrogen bonds. STM observations made on these two molecules showed that the concepts of isoreticular networks with tunable pore size and tendency for

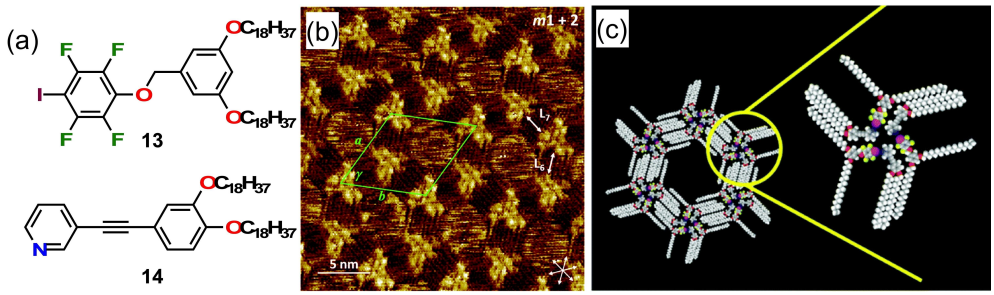


**Figure 8.** (a) Molecular structures of the alkoxy substituted halogen bond donating (**13**) and accepting building blocks (**14**). (b) STM image of the porous two component self-assembled network sustained by C–I···N halogen bonds and the van der Waals interactions between the alkoxy chains. (c) Molecular model showing self-assembled motif. Reproduced from ref. [34] with permission from the Royal Society of Chemistry.

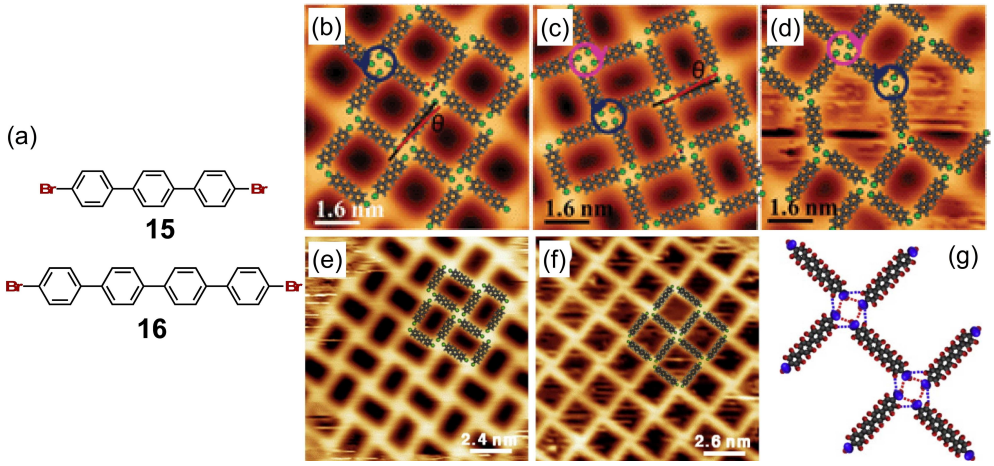


**Figure 9.** (a) Molecular structures of 4,4′′-dibromo-p-terphenyl (**15**) and 4,4′′-dibromo-p-quaterphenyl (**16**). (b–d) STM images of the monolayers formed by **15** on Ag(111) surface under UHV conditions at 80 K. Square (b), rectangular (c) and polygonal (d) motifs are formed based on $X_4$ or $X_3$-based synthons. (e, f) Self-assembled networks formed by **15** (e) and **16** (f) on the Au(111) surface under UHV conditions. (g) A schematic of the halogen and hydrogen bonding motif. Reproduced from ref. [35] and [36] with permission from the Royal Society of Chemistry and Elsevier B.V., respectively.

close-packing at higher coverage both apply to halogen-bonded assemblies.[36]

The degree of complexity of such assemblies can be increased by incorporating other (hetero)atoms in the molecules. The study of two different isomers of dibromoanthraquinones (**17**, **18** Figure 10a) at the UHV/Au(111) interface showed how the molecular design can influence the nature of the interactions and the arrangement of molecules within the network.[37] **17** forms an open network with square-shaped pores stabilized by a combination of hydrogen and halogen bonds between neighbouring molecules. Quadruple nodes based on $X_4$ synthons similar to those described earlier are formed. DFT-based molecular modelling revealed that the network is stabilized *via* Br···Br halogen bonds and O···H and Br···H hydrogen bonds. **18** on the other hand yielded a close-packed chevron structure on the gold surface. This network is also stabilized by a mix of hydrogen and halogen bonding but there, a Br atom only forms a halogen bond with an O atom (while still forming hydrogen bonds with two H atoms), showing that the nature of the halogen bonds formed can be controlled by position of Br atoms on the molecule. The distances of the intermolecular bonds formed by the two

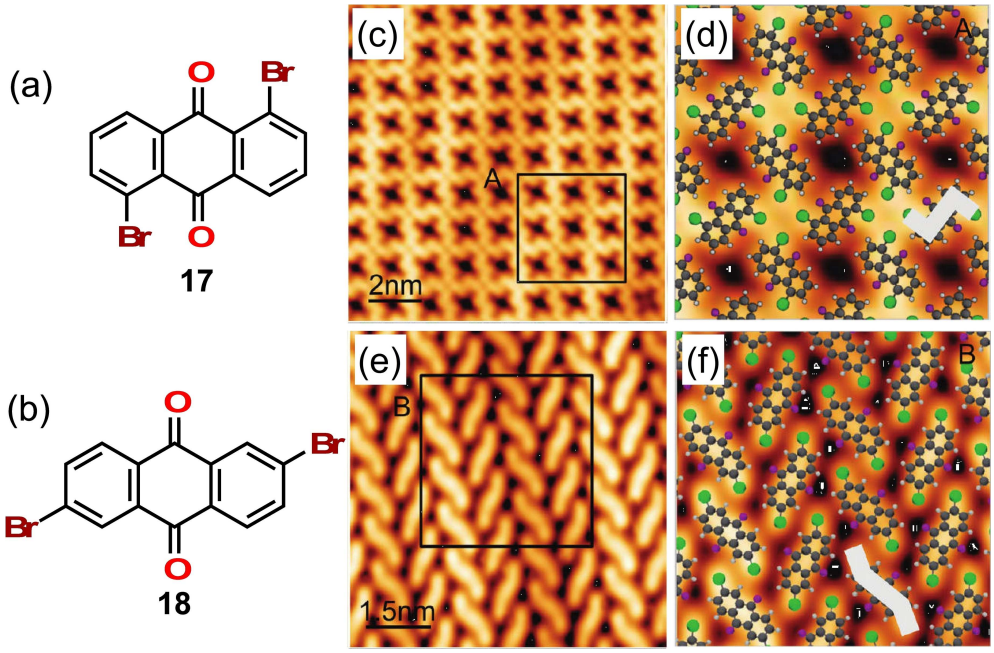


**Figure 10.** (a, b) Molecular structures of the isomeric dibromoanthraquinones derivatives **17** and **18**. (c, d) STM images of the network formed by **17** at the UHV/Au(111) interface. (e, f) STM images of the network formed by **18** at the UHV/Au(111) interface. Molecular models corresponding to the self-assembled networks are overlaid on the images presented in panels (d) and (f). Reproduced from ref. [37] with permission from the American Chemical Society.

isomers are close to the sum of the van der Waals radii of their atoms, meaning the bonds are relatively weak. However, they are quite similar to the distances of the same type of bonds measured in bulk under similar molecular environments (*i.e.* atoms covalently bonded to C atoms).[37] Similar quadruple nodes based on $X_4$ synthons have been reported for self-assembly of brominated pyrenes on Au(111) under UHV conditions.[31]

The fact the chlorine-chlorine type II contacts are weak was demonstrated in a follow up study involving 1,5 dichloroanthraquinone, in which the bromine atoms of **17** (Figure 10a) are replaced by chlorine. While the square-shaped polymorph formed by the chlorinated analogue was found to be similar to that of the brominated one, DFT calculations revealed that the Cl···Cl contacts were longer than the sum of their van der Waals radii indicating weak interactions. The Cl···H hydrogen bonds as anticipated were relatively stronger. The chlorinated analogue also formed the chevron type close-packed network which is sustained solely by Cl···H hydrogen bonds without any Cl···Cl contacts. This phase was found to form exclusively upon annealing the surface thus indicating its superior thermodynamic stability. This comparative study illustrated that hydrogen bonding interactions and close packing considerations overrule relatively weak halogen-halogen interactions such as the Cl–Cl type II contacts.[38]

Halogen-halogen type-II contacts have been recently employed to generate exotic supramolecular architectures such as fractals. Fractals are complex patterns that are self-similar across different length scales. These complex yet fascinating patterns are routinely observed in nature and are considered important in science, mathematics and engineering. Sierpiński triangles represent a prototypical fractal pattern and consist of an equilateral triangle which is recursively subdivided into smaller equilateral triangles (Figure 11b). Fabricating such repetitive patterns has proven to be notoriously difficult and synthetic fractal patterns are often defective.

A brominated molecule featuring a 120° bend in the backbone, namely 4,4‴-dibromo-1,1′:3′,1″:4″,1‴-quaterphenyl (**19**, Figure 11a), was used as the building block for realizing the assembly of Sierpiński triangles on Ag(111). **19** was brought to the Ag(111) surface using vapor phase deposition. Fast cooling of the surface to 4.4 K lead to spontaneous self-assembly of defect-free Sierpiński triangles. Figure 11c shows STM images showing the silver surface exclusively covered with equilateral triangular features closely resembling the fractal pattern. Although theoretically such fractals can be infinite, Sierpiński triangles up to fourth order (n = 4) were observed on the surface (Figure 11b, c). The primary unit of the assembled network consists of three molecules of **19** assembled together *via* Br···Br contacts reminiscent of the $X_3$ synthons. The cyclic arrangement of Br atoms relative to each other was found to be either clockwise (CW) or counterclockwise (CCW) leading to the expression of organizational chirality within the fractal assembly (Figure 11d, e). As described earlier for other examples, this network is stabilized by type-II halogen-halogen interactions and also by weak hydrogen bonding between the Br atom of one molecule with the α-H atom of the adjacent molecule (Figure 11f).[39]

The remarkably ordered fractal pattern with the largest triangle (n = 4) consists of nearly 300 molecules. This complex assembly is the result of a combination of factors including molecular design, choice of the substrate, precise experimental

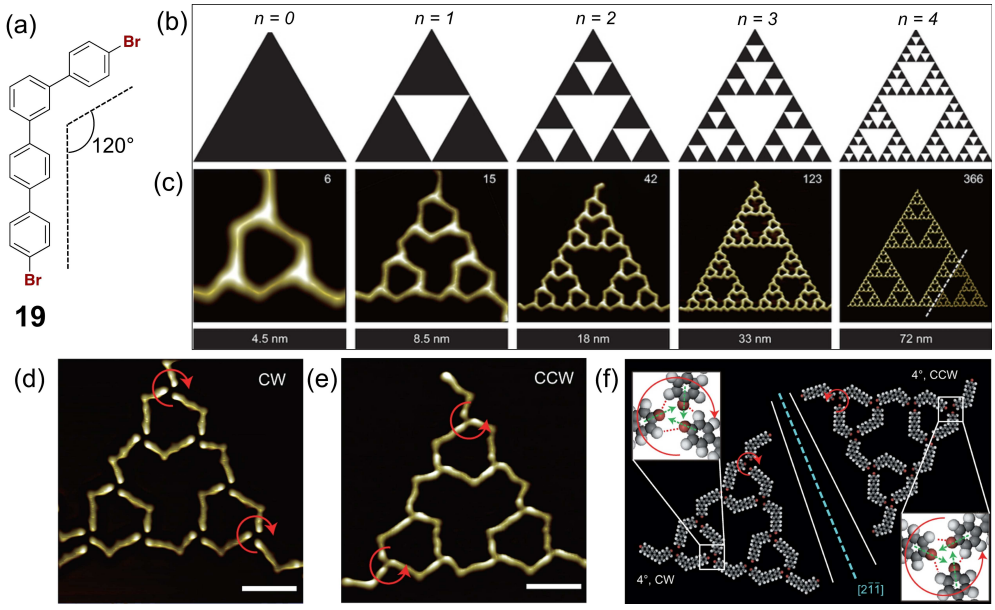


**Figure 11.** (a) Molecular structure of **19**. (b) Simple models of Sierpiński triangles. (c) STM images of self-assembled Sierpiński triangles formed on Ag (111). The numbers provided in the upper right corner of each STM image indicate the number of molecules involved in the assembly. (d and e) STM images showing enantiomorphous Sierpiński triangles. Scale bar = 2 nm. (f) Molecular models corresponding to STM images provided in panels (d) and (e) showing the $X_3$ synthon with Br···Br type-II contacts further supported by hydrogen bonds. Reproduced from ref. [39] with permission from the Nature Publishing Group.

conditions in terms of temperature control and weak yet directional supramolecular interactions. These factors collectively allow correction errors during the assembly process and reduce the number defects. Each node in the triangle is precisely defined thanks to the $X_3$ synthon, which is also in perfect registry with the underlying lattice of silver. The asymmetric design of the building block ensured minimal defect density. In case a molecule is incorporated into the assembly with its 'wrong' end, the opposite end of the molecule is incapable of forming a stable node. Such defects were eventually removed during the annealing process.[39]

An interesting development is the imaging of halogenated aromatic molecules using STM with carbon monoxide modified tips. These experiments are typically carried out on metal surfaces at cryogenic temperatures under UHV conditions. Recent years have witnessed increased activity in the field of scanning probe microscopy imaging of organic adsorbates using such modified tips as it provides comparable or better resolution than standard STM under similar conditions. Modified tips can be used during both STM and AFM experiments. This method has allowed acquisition of extremely high-resolution images of organic molecules.[40]

Scanning probe microscopy carried out using CO modified tips has been recently employed for imaging perfluorinated aromatic molecules on metal surfaces. We note that the general ability of this advanced microscopy technique to image intermolecular interactions is being debated within the scanning probe microscopy community.[41] Notwithstanding the debate, in the following we describe a couple of examples where fluorinated systems were imaged and the evidence of halogen-halogen contacts in the STM/AFM images was sought. The first example involves the self-assembly of a perfluorinated phenyleneethynylene derivative (**20**, Figure 12a) on Ag(111) surface characterized using STM and AFM with CO modified tips. While studying the co-assembly of **20** and its non-fluorinated analogue, bond-like features were observed in AFM images at positions where the fluorine-fluorine contacts are expected (Figure 12b, c). Independent AFM experiments on the self-assembly of **20** alone revealed a close-packed monolayer in which the molecules interact with each other *via* a trimeric contact reminiscent of the $X_3$ synthon (Figure 12d, e). Analysis of the AFM images revealed that C–F···F–C bond angles to be 120° which is consistent with the $X_3$ synthon. However, the distance between the fluorine atoms was found to be 300 pm which is larger than the sum of van der Waals radii of the fluorine atoms. This indicates that halogen bonds are absent in these assemblies.[42]

In a relatively recent article, a more definitive claim about imaging of halogen bonds was made. STM imaging of hexafluoro- and hexabromobenzene (**21, 22** Figure 13a) was carried out on Ag(110) surface using a modified variant of the technique that employs an inelastic tunnelling probe (itProbe) with a CO-functionalized tip. In this approach, the lateral vibrations of the CO molecule attached to the tip serve as a probe of the gradient of lateral forces exerted on the CO molecule, yielding STM contrast. Figure 13c shows an STM image of **21** where the molecules are arranged in a hexagonal close packed arrangement. The intermolecular contacts consist of trimeric nodes where each fluorine atom is involved in a triangular arrangement with fluorine atoms of two neighbouring molecules (Figure 13d). Once again, this geometry is reminiscent of the $X_3$ synthon however the C–F···F bond angles

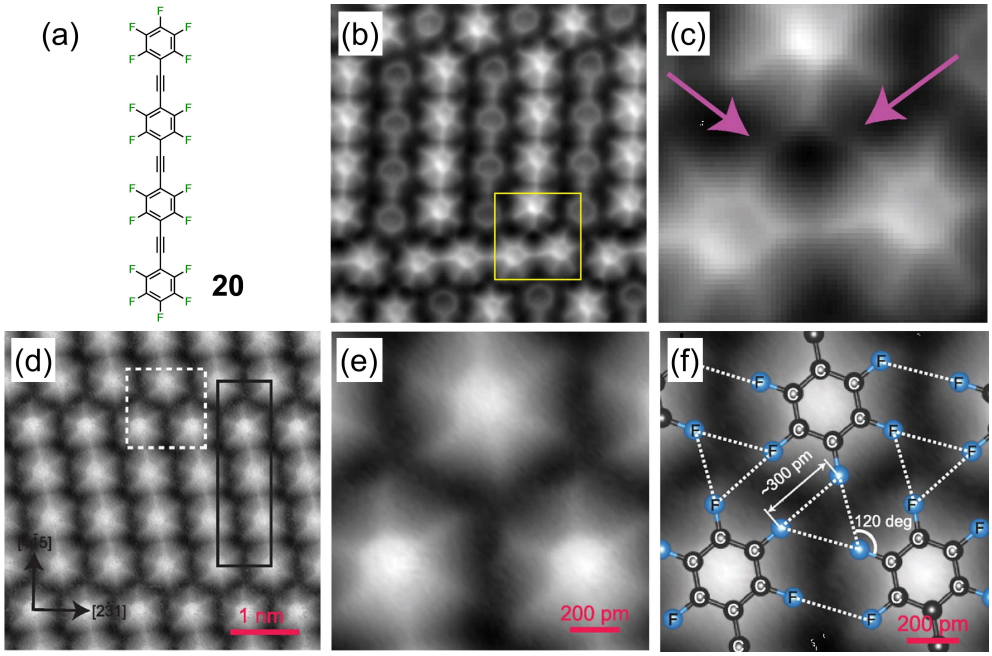


**Figure 12.** (a) Molecular structure of **20**. (b) Frequency shift map of the self-assembled monolayer of **20** and its non-fluorinated analogue on the Ag(111) surface. The image was obtained at 4.8 K using a CO modified tip. (c) Magnified image from the area represented by the yellow square in (b). (d) Frequency shift map of the self-assembled monolayer of **20**. (e) Magnified image from the area represented by square in (d). (f) Panel (e) with overlaid schematic of the molecules with interatomic distances and angles. Reproduced from ref. [42] with permission from the American Chemical Society.

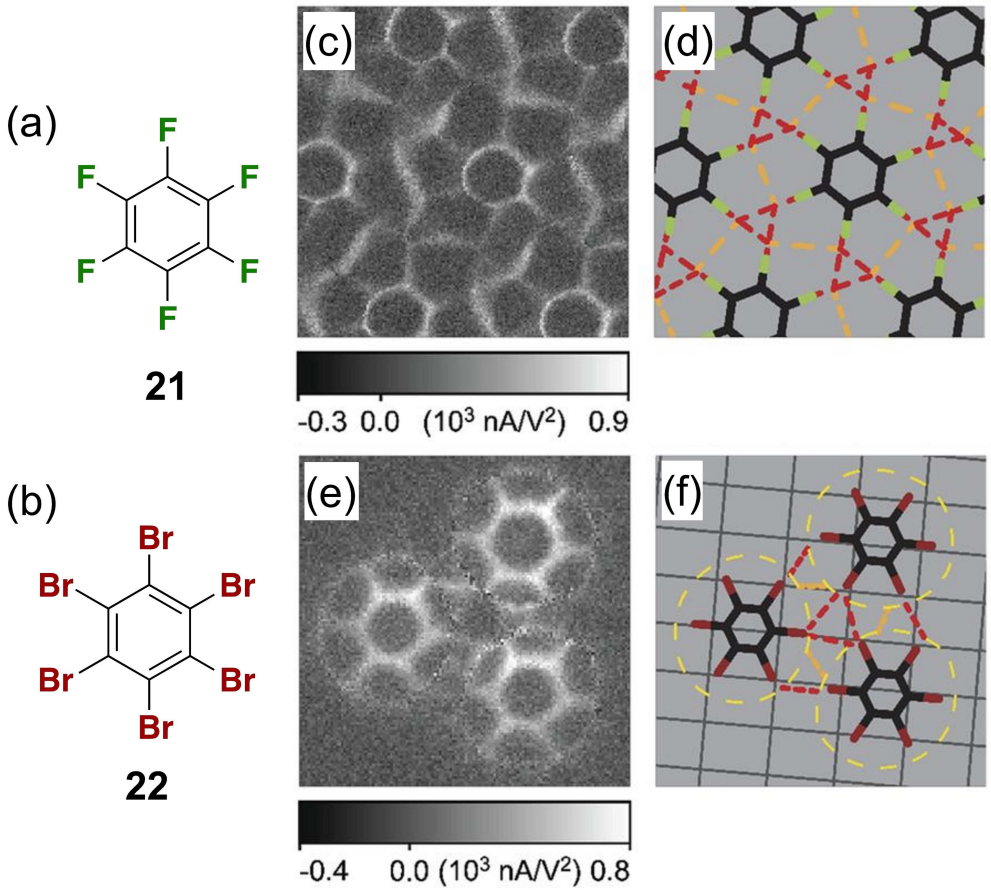


**Figure 13.** (a, b) Molecular structure of **21** and **22**, respectively. (c) Constant current itProbe STM image showing the monolayer of **21**. (d) Schematic showing the arrangement of molecules of **21** in the STM image presented in (e). Constant current itProbe STM image showing the monolayer of **22**. (f) Schematic showing the arrangement of molecules of **22** in the STM image presented in (e). Reproduced from ref. [43] with permission from the American Association for the Advancement of Science.

were found to deviate from the expected value of 180°. This deviation was attributed to the molecule-substrate registry which forces the molecules to sit atop the short bridge site on the Ag(110) surface and orient two of its C–F bonds along a particular crystallographic direction. Control experiments carried out using **22**, in which case the bromine atoms are expected to form halogen bonds, revealed the formation of trimers of molecules organized in a fashion similar to that of **21** (Figure 13e, f). Based on the similarities of the two motifs, it was concluded that the features observed in between the molecules arise due to halogen bonds. First-principles DFT calculations were able to reproduce the experimentally observed rotational angles and overall geometry. However, these calculations were carried out on freestanding monolayers in vacuum and the influence of the underlying substrate was not taken into account.[43]

While the issues surrounding the interpretation of the sub- and intermolecular image contrast obtained using CO-modified tips continues to be debated, we note that the limitations of the technique are far from clearly understood. Recent reports have indicated that the flexibility of the CO tip, rather than the presence of an intermolecular bond, determines whether or not such intermolecular features are observed, suggesting that the assignment of such features should be done with great discretion.[44] Although AFM and STM with modified tips cannot be used to assign the presence or absence of intermolecular bonds, the high resolution achieved in these attempts bodes well for understanding intermolecular interactions as it allows to precisely determine the exact location, separation and orientation of (halogen) atoms within a molecule that forms a 2D matrix.

Similar to the case of solution/solid interface, examples of self-assembled networks sustained by halogen-heteroatom contacts are rare also at the UHV/solid interface. One such case is the self-assembly of 3,10-dibromo-perylo[1,12-b,c,d] thiophene (**22**, Figure 14a) on Ag(111).[45] **22** is a polycyclic aromatic hydrocarbon with $C_2v$ symmetry possessing bromine atoms on the two sides of its perylene core and a sulphur pointing orthogonally to the axis formed by the Br atoms.

It was found to form three different polymorphs (PN1, PN2 and PN3, Figures 14b–d) at 77 K on Ag(111). Polymorph PN1 is a honeycomb network sustained by Br···Br interactions *via* the $X_3$ synthon. PN2 consists of a kagome network stabilized by Br···S and Br···H interactions. The PN3 network exhibits a complex structure as it is somewhat a mix of PN1 and PN2 and is stabilized by the three types of interactions mentioned earlier.

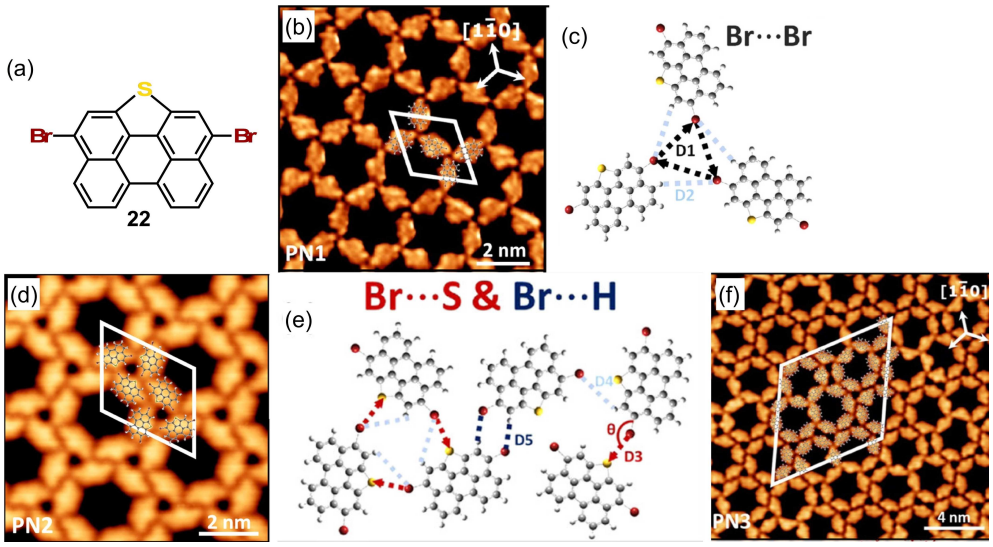


**Figure 14.** (a) Molecular structure of **22**. (b), (d), and (f) show respectively the STM images of the PN1, PN2 and PN3 polymorphs formed by **22** at the UHV/Ag (111) interface. (c) and (e) show the different types of interactions that stabilize the three polymorphs. Reproduced from ref. [45] with permission from the American Chemical Society.

The unit cell of PN3 is composed of 36 molecules. DFT calculations carried out on the trimeric motif indicated higher stability for PN1 than PN2. The Br···Br interaction was found to be stronger than the Br···S one due to the higher electronegativity of Br. Despite the lower stability inferred from DFT calculations, annealing of the surface led to an increase in the surface coverage of PN2 to 100% with complete disappearance of PN1 and PN3, suggesting higher stability for PN2. This apparent contradiction can be understood by considering the following two factors. First, the molecular density of the three polymorphs changes as: PN2 (0.636 $nm^{-2}$) > PN3 (0.618 $nm^{-2}$) > PN1 (0.512 $nm^{-2}$). However, the higher density of PN2 can only partially explain its stability. This is because PN2 was formed exclusively at low surface coverage of **22**. Secondly, DFT calculations performed on PN1 and PN2 (without the Ag surface) revealed that PN2 is indeed more stable (−2.97 kcal/mol vs −1.75 kcal/mol) due to the multiplicity of intermolecular interactions (*i.e.* Br···H and van der Waals interactions that are not present in PN1).[45]

Another example where halogen-halogen and halogen-heteroatom interactions defined the supramolecular networks consists of the self-assembly of two structurally similar molecules, namely 3,9-dibromodinaphtho[2,3-b:2′,3′-d]thiophene (**23**, Figure 15a) and [3,9-dibromodinaphtho[2,3-b:2′,3′-d]furan (**24**, Figure 15b).[46] The self-assembled networks were investigated on Ag(111) at 4.8 K using STM and non-contact AFM. The difference between the two molecules is the presence of either thiophene or the furan moieties within their structures. The two heteroatoms namely S and O exhibit respectively a neutral and negative electrostatic potential (Figure 15a, b). **23** formed a single walled porous network whereas **24** was found to form a nanoporous network with double walls. The single walled network of **23** is stabilized by type-II Br···Br interactions *via* an $X_3$ synthon. On the other hand, the negative electrostatic potential on the O atom in **24** gave rise to a more complex structure stabilized by nodes involving three molecules assembled by Br···Br and Br···O halogen bonds. This subtle difference between the assembly of the two similar derivatives was used to create two nanoporous networks with identical pore size but different interpore distances (respectively one and two molecules in the wall). It was thus considered as a model system to study arrays of quantum dots (the nanopores in that case) and engineer their tunable barrier width. By maintaining overall interdot coupling, it becomes possible to generate two-dimensional electron gases.[46]

## 4. Conclusions

Halogen bonding has emerged as a promising tool in the toolbox of supramolecular chemists and crystal engineers. 2D crystal engineering represents a small yet significant branch in the larger field of supramolecular chemistry where halogen bonds are being increasingly used for creating complex self-assembled architectures. A review of the literature presented above shows that the real potential of halogen bonding in on-surface supramolecular chemistry is yet to be realized. It appears that in cases where halogen bonds are targeted, especially in the case of 2D crystal engineering at the solution/solid interface, their influence on the final structural outcome is rather small and it can often be questioned if they are indeed structure directing similar to hydrogen bonds. To ensure fabrication of networks truly defined by halogen bonds, significant efforts need to be put in the design aspect of 2D crystal engineering. As evident from the survey presented above, in most cases, the halogen bonds are accompanied by concomitantly formed hydrogen bonds involving the halogen atoms, indicating that the halogen-halogen contacts/bonds

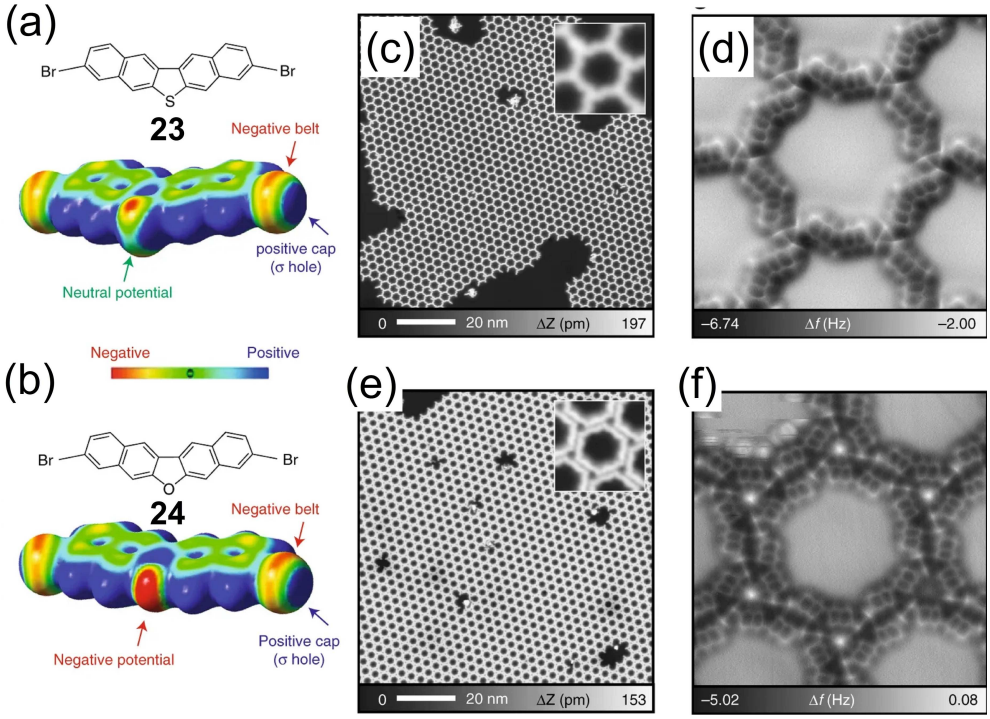


**Figure 15.** (a), (b) Molecular structures and the electrostatic potential maps of **23** and **24**, respectively. (c), (e) Large scale STM images of the networks formed by **23** and **24**, respectively. (d), (f) High-resolution non-contact AFM images for self-assembled motifs of **23** and **24**, respectively. Reproduced from ref. [46] with permission from the Nature publishing group.

may simply arise due to global considerations pertaining intermolecular and interfacial interactions. Another factor is the dominance of molecule-substrate interactions on self-assembled network formation which complicates the quantification of the real contribution of halogen bonding to the stabilization of the supramolecular networks.

Halogen bonded assemblies obtained under UHV environment represent a rather simple and clean scenario where the structure directing ability of halogen bonds can be tested. The STM and AFM measurements carried out using CO modified tips represent a significant development, where the X-bonded nodes can be imaged at high resolution. Although the interpretation of the intermolecular contrast and the ability to image intermolecular (halogen) bonds is under scrutiny, the high resolution achieved using these techniques will allow precise determination of interatomic distances and angles thus allowing better insight into halogen bonding and halogen-halogen interactions.

## Acknowledgment

*The authors gratefully acknowledge financial support from the Fund of Scientific Research Flanders (FWO), KU Leuven – Internal Funds. This work was in part supported by FWO under EOS 30489208.*

## Conflict of Interest

The authors declare no conflict of interest.

**Keywords:** halogen bonding · halogen-halogen interactions · 2D crystal engineering · scanning tunneling microscopy · self-assembly

[1] a) K. S. Mali, N. Pearce, S. De Feyter, N. R. Champness, *Chem. Soc. Rev.* **2017**, *46*, 2520; b) A. G. Slater, P. H. Beton, N. R. Champness, *Chem. Sci.* **2011**, *2*, 1440; c) A. Ciesielski, C.-A. Palma, M. Bonini, P. Samorì, *Adv. Mater.* **2010**, *22*, 3506.
[2] J. A. A. W. Elemans, S. Lei, S. De Feyter, *Angew. Chem. Int. Ed.* **2009**, *48*, 7298.
[3] S. M. Barlow, R. Raval, *Surf. Sci. Rep.* **2003**, *50*, 201.
[4] a) P. Muller-Buschbaum, *Polym. J.* **2013**, *45*, 34; b) P. Müller-Buschbaum, *Adv. Mater.* **2014**, *26*, 7692.
[5] T. Arnold, S. M. Clarke, *Curr. Opin. Colloid Interface Sci.* **2012**, *17*, 23.
[6] D. P. Goronzy, M. Ebrahimi, F. Rosei Arramel, Y. Fang, S. De Feyter, S. L. Tait, C. Wang, P. H. Beton, A. T. S. Wee, P. S. Weiss, D. F. Perepichka, *ACS Nano* **2018**, *12*, 7445.
[7] a) M. Lackinger, W. M. Heckl, *Langmuir* **2009**, *25*, 11307; b) A. G. Slater, L. M. A. Perdigão, P. H. Beton, N. R. Champness, *Acc. Chem. Res.* **2014**, *47*, 3417.
[8] a) K. Tahara, S. Lei, J. Adisoejoso, S. De Feyter, Y. Tobe, *Chem. Commun.* **2010**, *46*, 8507; b) H. Ascolani, M. W. van der Meijden, L. J. Cristina, J. E. Gayone, R. M. Kellogg, J. D. Fuhr, M. Lingenfelder, *Chem. Commun.* **2014**, *50*, 13907.
[9] a) P. B. Weber, R. Hellwig, T. Paintner, M. Lattelais, M. Paszkiewicz, P. Casado Aguilar, P. S. Deimel, Y. Guo, Y.-Q. Zhang, F. Allegretti, A. C. Papageorgiou, J. Reichert, S. Klyatskaya, M. Ruben, J. V. Barth, M.-L. Bocquet, F. Klappenberger, *Angew. Chem. Int. Ed.* **2016**, *55*, 5754; b) L. Dong, Z. A. Gao, N. Lin, *Prog. Surf. Sci.* **2016**, *91*, 101.

[10] a) M. K. Kim, Y. Xue, T. Paskova, M. B. Zimmt, *Phys. Chem. Chem. Phys.* **2013**, *15*, 12466; b) Y. Wei, W. Tong, M. B. Zimmt, *J. Am. Chem. Soc.* **2008**, *130*, 3399.
[11] a) Y. He, J. Kröger, Y. Wang, *ChemPhysChem* **2017**, *18*, 429; b) Z. Guo, K. Tahara, K. Inukai, H. Takeda, M. Kouno, K. Iritani, Y. Tobe, *J. Phys. Chem. C* **2015**, *119*, 15977.
[12] a) C. Arrigoni, G. Schull, D. Bléger, L. Douillard, C. Fiorini-Debuisschert, F. Mathevet, D. Kreher, A.-J. Attias, F. Charra, *J. Phys. Chem. Lett.* **2009**, *1*, 190; b) D. Bléger, D. Kreher, F. Mathevet, A.-J. Attias, G. Schull, A. Huard, L. Douillard, C. Fiorini-Debuischert, F. Charra, *Angew. Chem. Int. Ed.* **2007**, *46*, 7404.
[13] R. Desiraju Gautam, P. S. Ho, L. Kloo, C. Legon Anthony, R. Marquardt, P. Metrangolo, P. Politzer, G. Resnati, K. Rissanen, *Definition of the halogen bond (IUPAC Recommendations 2013), Vol. 85* **2013**, p. 1711.
[14] a) M. H. Kolář, P. Hobza, *Chem. Rev.* **2016**, *116*, 5155; b) T. Clark, M. Hennemann, J. S. Murray, P. Politzer, *J. Mol. Model.* **2007**, *13*, 291.
[15] A. Kovács, Z. Varga, *Coord. Chem. Rev.* **2006**, *250*, 710.
[16] G. Cavallo, P. Metrangolo, R. Milani, T. Pilati, A. Priimagi, G. Resnati, G. Terraneo, *Chem. Rev.* **2016**, *116*, 2478.
[17] P. Metrangolo, J. S. Murray, T. Pilati, P. Politzer, G. Resnati, G. Terraneo, *Cryst. Growth Des.* **2011**, *11*, 4238.
[18] V. R. Pedireddi, D. S. Reddy, B. S. Goud, D. C. Craig, A. D. Rae, G. R. Desiraju, *J. Chem. Soc. Perkin Trans. 1* **1994**, 2353.
[19] a) Q.-Z. Li, B. Jing, R. Li, Z.-B. Liu, W.-Z. Li, F. Luan, J.-B. Cheng, B.-A. Gong, J.-Z. Sun, *Phys. Chem. Chem. Phys.* **2011**, *13*, 2266; b) M. Domagała, A. Lutyńska, M. Palusiak, *J. Phys. Chem. A* **2018**, *122*, 5484.
[20] C. C. Robertson, J. S. Wright, E. J. Carrington, R. N. Perutz, C. A. Hunter, L. Brammer, *Chem. Sci.* **2017**, *8*, 5392.
[21] A. M. S. Riel, R. K. Rowe, E. N. Ho, A.-C. C. Carlsson, A. K. Rappé, O. B. Berryman, P. S. Ho, *Acc. Chem. Res.* **2019**, *52*, 2870.
[22] R. Gutzler, O. Ivasenko, C. Fu, J. L. Brusso, F. Rosei, D. F. Perepichka, *Chem. Commun.* **2011**, *47*, 9453.
[23] R. Gutzler, C. Fu, A. Dadvand, Y. Hua, J. M. MacLeod, F. Rosei, D. F. Perepichka, *Nanoscale* **2012**, *4*, 5965.
[24] R. Gatti, J. M. MacLeod, J. A. Lipton-Duffin, A. G. Moiseev, D. F. Perepichka, F. Rosei, *J. Phys. Chem. C* **2014**, *118*, 25505.
[25] a) X. Shen, X. Wei, P. Tan, Y. Yu, B. Yang, Z. Gong, H. Zhang, H. Lin, Y. Li, Q. Li, Y. Xie, L. Chi, *Small* **2015**, *11*, 2284; b) S. Ahn, A. J. Matzger, *J. Am. Chem. Soc.* **2010**, *132*, 11364; c) S. Lei, K. Tahara, F. C. De Schryver, M. Van der Auweraer, Y. Tobe, S. De Feyter, *Angew. Chem. Int. Ed.* **2008**, *47*, 2964.
[26] a) R. Gutzler, T. Sirtl, J. r F. Dienstmaier, K. Mahata, W. M. Heckl, M. Schmittel, M. Lackinger, *J. Am. Chem. Soc.* **2010**, *132*, 5084; b) A. Mukherjee, J. Teyssandier, G. Hennrich, S. De Feyter, K. S. Mali, *Chem. Sci.* **2017**, *8*, 3759.
[27] F. Silly, J. Phys, *Chem. C* **2017**, *121*, 10413.
[28] E. Bosch, C. L. Barnes, *Cryst. Growth Des.* **2002**, *2*, 299.
[29] D. Peyrot, M. G. Silly, F. Silly, *Phys. Chem. Chem. Phys.* **2018**, *20*, 3918.
[30] X. Hu, B. Zha, Y. Wu, X. Miao, W. Deng, *Phys. Chem. Chem. Phys.* **2016**, *18*, 7208.
[31] T. A. Pham, F. Song, M.-T. Nguyen, M. Stöhr, *Chem. Commun.* **2014**, *50*, 14089.
[32] A. Mukherjee, A. Sanz-Matias, G. Velpula, D. Waghray, O. Ivasenko, N. Bilbao, J. N. Harvey, K. S. Mali, S. De Feyter, *Chem. Sci.* **2019**, *10*, 3881.
[33] Q.-N. Zheng, X.-H. Liu, T. Chen, H.-J. Yan, T. Cook, D. Wang, P. J. Stang, L.-J. Wan, *J. Am. Chem. Soc.* **2015**, *137*, 6128.
[34] Y. Kikkawa, M. Nagasaki, E. Koyama, S. Tsuzuki, K. Hiratani, *Chem. Commun.* **2019**, *55*, 3955.
[35] K.-H. Chung, J. Park, K. Y. Kim, J. K. Yoon, H. Kim, S. Han, S.-J. Kahng, *Chem. Commun.* **2011**, *47*, 11492.
[36] W. J. Jang, K.-H. Chung, M. W. Lee, H. Kim, S. Lee, S.-J. Kahng, *Appl. Surf. Sci.* **2014**, *309*, 74.
[37] J. K. Yoon, W. -j Son, K.-H. Chung, H. Kim, S. Han, S.-J. Kahng, *J. Phys. Chem. C* **2011**, *115*, 2297.
[38] S.-K. Noh, J. H. Jeon, W. J. Jang, H. Kim, S.-H. Lee, M. W. Lee, J. Lee, S. Han, S.-J. Kahng, *ChemPhysChem* **2013**, *14*, 1177.
[39] J. Shang, Y. Wang, M. Chen, J. Dai, X. Zhou, J. Kuttner, G. Hilt, X. Shao, J. M. Gottfried, K. Wu, *Nat. Chem.* **2015**, *7*, 389.
[40] L. Gross, F. Mohn, N. Moll, P. Liljeroth, G. Meyer, *Science* **2009**, *325*, 1110.
[41] S. P. Jarvis, *Int. J. Mol. Sci.* **2015**, *16*, 19936.
[42] S. Kawai, A. Sadeghi, F. Xu, L. Peng, A. Orita, J. Otera, S. Goedecker, E. Meyer, *ACS Nano* **2015**, *9*, 2574.
[43] Z. Han, G. Czap, C. -l Chiang, C. Xu, P. J. Wagner, X. Wei, Y. Zhang, R. Wu, W. Ho, *Science* **2017**, *358*, 206.
[44] a) P. Hapala, G. Kichin, C. Wagner, F. S. Tautz, R. Temirov, P. Jelínek, *Phys. Rev. B* **2014**, *90*, 085421; b) P. Hapala, R. Temirov, F. S. Tautz, P. Jelínek, *Phys. Rev. Lett.* **2014**, *113*, 226101; c) S. K. Hämäläinen, N. van der Heijden, J. van der Lit, S. den Hartog, P. Liljeroth, I. Swart, *Phys. Rev. Lett.* **2014**, *113*, 186102.
[45] L. Xing, W. Jiang, Z. Huang, J. Liu, H. Song, W. Zhao, J. Dai, H. Zhu, Z. Wang, P. S. Weiss, K. Wu, *Chem. Mater.* **2019**, *31*, 3041.
[46] I. Piquero-Zulaica, J. Lobo-Checa, A. Sadeghi, Z. M. A. El-Fattah, C. Mitsui, T. Okamoto, R. Pawlak, T. Meier, A. Arnau, J. E. Ortega, J. Takeya, S. Goedecker, E. Meyer, S. Kawai, *Nat. Commun.* **2017**, *8*, 787.

Manuscript received: November 14, 2019
Revised manuscript received: January 14, 2020